J. Fluid Mech. (2022), *vol*. 935, A27, doi:10.1017/jfm.2022.20

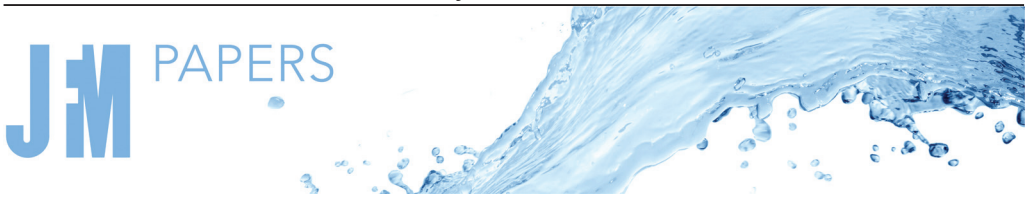

A model for bubble dynamics in a protein solution

Xiaoxu Zhong[1] **and Arezoo M. Ardekani**[1],†

[1]School of Mechanical Engineering, Purdue University, West Lafayette, IN 47906, USA

(Received 18 September 2021; revised 6 December 2021; accepted 5 January 2022)

This paper presents a model for bubble dynamics in a protein solution, including varying surface tension and dynamic adsorption/desorption of protein onto the bubble surface. We model the protein-coated bubble surface as a linear viscoelastic interface. Two cases are studied to understand the importance of the surface excess stress: (1) bubble dissolution in a protein solution due to gas diffusion; and (2) bubble response to an imposed fluctuating pressure field. In the first case study, the surface excess stress stabilizes the bubble against dissolution. Initially, the surface excess stress is negligible, and the dissolution rate is governed by the Weber number, which compares the gas inertial force and the surface tension force. As the bubble shrinks, the surface excess stress grows and eventually balances the surface tension. After that, the dissolution rate is governed by the protein desorption rate and the elasto-capillary number, which compares the surface tension and the surface dilatational elasticity. Our model predictions for the dissolution process agree with experiments before the bubble buckles. In the second case study, the surface dilatational viscosity and dilatational elasticity add resistance and stiffness to the system, respectively. Including the surface excess stress increases (or reduces) the amplitude of the bubble radius if the frequency of the imposed fluctuating pressure is greater (or less) than a critical value. These results highlight the importance of the surface rheology on the protein-coated bubble dynamics, which has applications in drug delivery and ultrasound contrast agents.

Key words: bubble dynamics, cavitation, viscoelasticity

1. Introduction

Bubbles widely exist in nature, such as the ocean, volcanoes (Lyons *et al.* 2019) and trees (Vincent *et al.* 2012). Bubbles have many important applications in food science, medicine, chemical engineering, pharmaceutical engineering, etc. For instance, collapsing bubbles

† Email address for correspondence: ardekani@purdue.edu

generate shock waves and high-speed microjets towards a solid boundary; these properties have been used to clean food, break ice (Cui *et al.* 2018) and break the cell membrane to deliver drugs (Brennen 2015). As champagne is poured into a glass, bubbles rise to the air–champagne interface and burst. The bursting bubbles eject droplets, enhancing the champagne's fragrance (Liger-Belair *et al.* 2009). Moreover, bubbles can be used to enhance mixing in microfluidic devices (Liu *et al.* 2002; Wang *et al.* 2009).

The dynamics of an uncoated spherical bubble in an incompressible Newtonian medium is well described by the Rayleigh–Plesset equation (Rayleigh 1917; Plesset 1949; Plesset & Prosperetti 1977), which takes into account the surface tension and the liquid viscosity. Based on the Rayleigh–Plesset equation, various models have been developed to include liquid compressibility (Keller & Miksis 1980; Prosperetti & Lezzi 1986), thermal effects (Plesset & Zwick 1954), non-equilibrium evaporation and condensation (Fujikawa & Akamatsu 1980; Zhong *et al.* 2020), viscoelastic media (Warnez & Johnsen 2015; Murakami *et al.* 2021) and surface rheology (Chatterjee & Sarkar 2003; Doinikov & Dayton 2007; Dollet, Marmottant & Garbin 2019). Cavitation in protein solutions is also frequently encountered in the pharmaceutical (Veilleux *et al.* 2018; Zhang *et al.* 2021) and food (Narsimhan 2016) industries. However, this problem is complex for the following reasons: (1) the bulk rheological properties of protein solutions are complicated (Sharma *et al.* 2011); (2) many proteins adsorb preferentially to the solution–air interface (Fainerman, Lucassen-Reynders & Miller 1998); (3) the surface tension varies with the protein concentration at the interface (Miller *et al.* 2000); (4) the surface of the protein-coated bubble is usually viscoelastic (Narsimhan 2016); and (5) protein conformation, aggregation and shedding may occur at the interface, which can lead to the buckling of the interface (Lin *et al.* 2016).

Current theoretical studies on bubble dynamics have covered the varying surface tension (Marmottant *et al.* 2005) and the rheological behaviours of the bulk medium (Warnez & Johnsen 2015). Some works (Chatterjee & Sarkar 2003) further treat the bubble surface as a Newtonian interface and characterize it by the Boussinesq–Scriven constitutive equation (i.e. the surface dilatational viscosity has been included for spherical bubble dynamics). The surface dilatational elasticity is also an important parameter of the protein-coated bubble surface, but it has received much less attention. Thus, we aim to derive a theoretical description of a linear viscoelastic bubble surface and investigate the importance of the surface rheology. To simplify the problem, we will consider a spherical bubble shape and neglect the protein conformation, aggregation and shedding.

We will use two cases to illustrate the importance of surface rheology. The first case in which we are interested is bubble dissolution in a protein solution. For a bubble in water, the gas concentration in the bubble is higher than that in water due to the existence of surface tension; thus, the gas in the bubble continuously flows out. Epstein & Plesset (1950) adopted a quasi-static approximation and derived a simple solution for the rate of bubble growth/dissolution, which has been experimentally validated (Kapodistrias & Dahl 2012). An uncoated microbubble in fresh water is expected to dissolve in seconds, but a bubble coated by lipids (Kwan & Borden 2012), proteins (Khan & Dalvi 2020), solid particles (Poulichet & Garbin 2015) or insoluble surfactants (Hanwright *et al.* 2005) can stay in the liquid for a long time (Kloek, van Vliet & Meinders 2001). We find that, for a bubble with a viscoelastic interface, the surface excess stress can balance the surface tension and thus stabilize the bubble against dissolution.

The second case in which we are interested is the response of a protein-coated bubble to an imposed fluctuating pressure field. Including both gas diffusion and the imposed pressure field – also known as rectified mass diffusion (Crum 1984; Church 1988;

Peñas-López *et al.* 2016) – can lead to interesting results, such as the progressive growth or reduction of the oscillation. Still, the problem becomes complicated, which brings difficulties in understanding the role of surface rheology. Thus, we will neglect gas diffusion in this second case. We will focus on the resonance between the bubble and an imposed acoustic pressure. In this case, theoretical solutions for resonant frequency and the peak amplitude of the bubble radius will be given.

This paper is organized as follows. A model for bubble dynamics in a protein solution is developed in § 2. The dissolution process of a protein-coated bubble is investigated in § 3. The response of a protein-coated bubble to an imposed fluctuating pressure is studied in § 4. Conclusions are provided in § 5.

2. Model

We consider a spherical bubble of radius R in an infinite domain of an incompressible protein solution. The origin of the spherical coordinate system is at the centre of the bubble; and r, θ and ϕ are the radial, azimuthal and polar coordinates, respectively. The system is spherically symmetric; thus, all physical quantities, such as the protein concentration in the bulk solution, are independent of θ and ϕ.

We let an overdot ($\dot{}$) denote the derivative with respect to time t; and v_r is the radial component of the liquid velocity. We consider a protein solution with a constant density ρ that is independent of the protein concentration. Coupling the mass conservation equation $\partial(r^2 v_r)/\partial r = 0$ and the boundary condition $v_r(r = R) = \dot{R}$, we get $v_r = \dot{R}R^2/r^2$. We model the protein solution as a Newtonian fluid, with its viscosity $\mu(c)$ depending on the local protein concentration $c(t, r)$. We let $\boldsymbol{\tau}$ denote the viscous stress tensor in the protein solution, so that $\tau_{rr} = -4\mu R^2\dot{R}/r^3$ and $\tau_{\theta\theta} = \tau_{\phi\phi} = -\tau_{rr}/2$. Substituting $v_r = \dot{R}R^2/r^2$ into the radial component of the momentum equation $\rho(\partial v_r/\partial t + v_r \partial v_r/\partial r) = -\partial p/\partial r + (\boldsymbol{\nabla}\cdot\boldsymbol{\tau})_r$, we have

$$\rho\left(\frac{R^2\ddot{R} + 2R\dot{R}^2}{r^2} - \frac{2R^4\dot{R}^2}{r^5}\right) = -\frac{\partial p}{\partial r} + (\boldsymbol{\nabla}\cdot\boldsymbol{\tau})_r, \tag{2.1}$$

where p is the pressure in the protein solution. We integrate the above equation from $r = R$ to $r \to \infty$, to obtain

$$\rho\left(R\ddot{R} + \frac{3}{2}\dot{R}^2\right) = p|_{r=R} - p_\infty + \int_R^\infty \frac{3\tau_{rr}}{r}\,\mathrm{d}r - \tau_{rr}|_{r=R}, \tag{2.2}$$

where p_∞ is the pressure in the protein solution far from the bubble.

The balance of the normal stress across the bubble surface is

$$p|_{r=R} - (\boldsymbol{\nabla}_s\cdot\boldsymbol{P}_s)\cdot\boldsymbol{n} - \tau_{rr}|_{r=R} = p_b. \tag{2.3}$$

Here $\boldsymbol{n}$ is the unit normal vector to the bubble surface; $p_b = p_v + p_g$ is the pressure inside the bubble, where p_v and p_g are the vapour pressure and gas pressure, respectively; $\boldsymbol{\nabla}_s \equiv \boldsymbol{I}_s\cdot\boldsymbol{\nabla}$ is the surface gradient operator; $\boldsymbol{I}_s \equiv \boldsymbol{I} - \boldsymbol{nn}$ is the surface identity matrix, where $\boldsymbol{I}$ is the identity matrix of size three; and $\boldsymbol{P}_s = \boldsymbol{I}_s\gamma + \boldsymbol{\tau}_s$ is the surface excess pressure tensor, where γ and $\boldsymbol{\tau}_s$ are the surface tension and surface excess stress tensor, respectively.

The constitutive equation for a linear viscoelastic interface (Edwards, Brenner & Wasan 1991; Narsimhan 2016) is

$$\boldsymbol{\tau}_s = \int_{-\infty}^{t} \{G^d(t-t') - G^s(t-t')\}(\boldsymbol{I}_s : \boldsymbol{D}_s(t'))\boldsymbol{I}_s \,\mathrm{d}t' + 2\int_{-\infty}^{t} G^s(t-t')\boldsymbol{D}_s(t')\,\mathrm{d}t', \quad (2.4)$$

where G^d and G^s are the dilatational modulus and the shear modulus, respectively. The surface rate-of-deformation tensor $\boldsymbol{D}_s$ is

$$\boldsymbol{D}_s \equiv \frac{1}{2}[(\nabla_s \boldsymbol{v}_s)\cdot \boldsymbol{I}_s + \boldsymbol{I}_s \cdot (\nabla_s \boldsymbol{v}_s)^{\mathrm{T}}] = \frac{\dot{R}}{r}\boldsymbol{I}_s, \quad (2.5)$$

where $\boldsymbol{v}_s$ is the surface velocity. Substituting (2.5) into (2.4) and coupling equations (2.2) and (2.3), we have

$$\rho\left(R\ddot{R} + \frac{3}{2}\dot{R}^2\right) = p_v + p_g - p_\infty - 12R^2\dot{R}\int_R^\infty \frac{\mu(c)}{r^4}\,\mathrm{d}r - \frac{2\gamma}{R} - \frac{4}{R}\int_{-\infty}^{t} G^d(t-t')\frac{\dot{R}(t')}{R(t')}\,\mathrm{d}t'. \quad (2.6)$$

We consider a linear viscoelastic interface, which is characterized by the Maxwell model

$$\frac{\partial}{\partial t}\left(\frac{\boldsymbol{\tau}_s}{E_s}\right) + \frac{\boldsymbol{\tau}_s}{\kappa_s} = \boldsymbol{D}_s, \quad (2.7)$$

where E_s and κ_s are the surface dilatational elasticity and the surface dilatational viscosity, respectively. Moreover, we assume E_s and κ_s to be proportional to the protein concentration at the interface Γ (Narsimhan 2016). Defining $E_s = E_{sl}\Gamma$ and $\kappa_s = \kappa_{sl}\Gamma$ and substituting them into (2.7), we have

$$\boldsymbol{\tau}_s = \int_{-\infty}^{t} \{E_s(t)\exp[-(t-t')/\lambda_s]\}\boldsymbol{D}_s(t')\,\mathrm{d}t', \quad (2.8)$$

where $\lambda_s = \kappa_s/E_s = \kappa_{sl}/E_{sl}$ is the (constant) relaxation time.

Thus, (2.6) for a linear viscoelastic bubble surface (characterized by the Maxwell model) can be rewritten as

$$\rho\left(R\ddot{R} + \frac{3}{2}\dot{R}^2\right) = p_v + p_g - p_\infty - 12R^2\dot{R}\int_R^\infty \frac{\mu(c)}{r^4}\,\mathrm{d}r - \frac{2\gamma}{R} - \frac{4E_s}{R}\int_0^t \exp[-(t-t')/\lambda_s]\frac{\dot{R}(t')}{R(t')}\,\mathrm{d}t', \quad (2.9)$$

or

$$\left.\begin{aligned} &\rho\left(R\ddot{R} + \frac{3}{2}\dot{R}^2\right) = p_v + p_g - p_\infty - 12R^2\dot{R}\int_R^\infty \frac{\mu(c)}{r^4}\,\mathrm{d}r - \frac{2\gamma}{R} - \frac{4E_s\mathcal{F}}{R}, \\ &\dot{\mathcal{F}} + \frac{\mathcal{F}}{\lambda_s} = \frac{\dot{R}}{R}, \quad \mathcal{F}|_{t=0} = 0, \end{aligned}\right\} \quad (2.10)$$

where $\mathcal{F} = \int_0^t \exp[-(t-t')/\lambda_s]\dot{R}(t')/R(t')\,\mathrm{d}t'$.

If we consider a constant liquid viscosity μ and a Newtonian bubble surface, i.e. $\lambda_s \to 0$, then (2.9) reduces to the model for surfactant- or lipid-coated bubbles (Chatterjee & Sarkar 2003; Marmottant *et al.* 2005):

$$\rho\left(R\ddot{R}+\frac{3}{2}\dot{R}^2\right)=p_v+p_g-p_\infty-4\mu\frac{\dot{R}}{R}-\frac{2\gamma}{R}-4\kappa_s\frac{\dot{R}}{R^2}. \tag{2.11}$$

If we consider a constant liquid viscosity μ and an elastic bubble surface, i.e. $\lambda_s \to \infty$, then (2.9) reduces to

$$\rho\left(R\ddot{R}+\frac{3}{2}\dot{R}^2\right)=p_v+p_g-p_\infty-4\mu\frac{\dot{R}}{R}-\frac{2\gamma}{R}-\frac{4E_s}{R}\ln\left(\frac{R}{R_0}\right), \tag{2.12}$$

where R_0 is the bubble radius at $t=0$.

The protein concentration in the bulk of the liquid, c with a unit kg m^{-3}, is governed by the advection–diffusion equation

$$\frac{\partial c}{\partial t}+v_r\frac{\partial c}{\partial r}=\frac{1}{r^2}\frac{\partial}{\partial r}\left(D_c r^2\frac{\partial c}{\partial r}\right), \tag{2.13}$$

which is subject to

$$c|_{t=0}=c_\infty, \quad c|_{r\to\infty}=c_\infty, \quad D_c\frac{\partial c}{\partial r}\bigg|_{r=R}=J, \tag{2.14a–c}$$

where D_c is the diffusion coefficient of protein in the bulk solution and c_∞ is the protein concentration far from the bubble surface. There are several well-accepted models (Henry, Langmuir, Frumkin, van der Waals, etc.) to describe the adsorption isotherms of surfactants and proteins. The corresponding expressions for the surface tension and adsorption/desorption flux can be found in the literature (Edwards *et al.* 1991; Manikantan & Squires 2020).

We model the net flux of protein to the interface J as

$$J=\begin{cases}\theta^a c_s(\Gamma_m-\Gamma)-\theta^d\Gamma, & \text{when } \Gamma\le\Gamma_m,\\ -\theta^d\Gamma, & \text{when } \Gamma>\Gamma_m.\end{cases} \tag{2.15}$$

Here θ^a and θ^d are the adsorption and desorption constants, respectively; $c_s=c|_{r=R}$ represents the protein concentration in the bulk solution close to the bubble surface; and Γ_m is the maximum packing density of protein at the bubble surface. If $\Gamma\le\Gamma_m$, the first term in J, which is described by the Langmuir equation (Craster, Matar & Papageorgiou 2009; Langevin 2014; Manikantan & Squires 2020), denotes the influx that is proportional to the protein concentration near the interface and the available space on the interface (proportional to $(\Gamma_m-\Gamma)$). The second term in J denotes the desorption of protein from the interface. If $\Gamma>\Gamma_m$, we assume the influx to be zero such that $J=-\theta^d\Gamma$.

The protein concentration at the bubble surface, Γ with a unit kg m^{-2}, is governed by (Stone 1990)

$$\frac{\mathrm{d}}{\mathrm{d}t}(\Gamma R^2) = JR^2. \tag{2.16}$$

We use the modified Langmuir relation (Fainerman *et al.* 1998) to characterize the surface tension:

$$\gamma = \begin{cases} \gamma_f + R_g T \Gamma_p \ln\left(1 - \dfrac{\Gamma}{\Gamma_m}\right), & \text{when } \Gamma \le \Gamma_c, \\ \gamma_c, & \text{when } \Gamma > \Gamma_c. \end{cases} \tag{2.17}$$

Here R_g, T, γ_f and γ_c are the gas constant, the temperature in the bulk solution near the interface, the surface tension of a clean solution–air interface, and the minimum surface tension, respectively; Γ_p is a fitting parameter, with unit mol m^{-2}; and $\Gamma_c = \Gamma_m - \Gamma_m \exp[(\gamma_c - \gamma_f)/(R_g T \Gamma_p)]$, beyond which the surface tension remains constant. Here $E_\Gamma \equiv -\Gamma \partial\gamma/\partial\Gamma$ is often called the Gibbs, Marangoni or simply dilatational modulus (Manikantan & Squires 2020); and E_Γ describes the rate of change of the surface tension with respect to the protein concentration on the bubble, while E_s and κ_s define the excess stress induced by the viscoelasticity of the interface. Thus, E_Γ and E_s (or κ_s) are two different parameters (Manikantan & Squires 2020). We use Mooney's equation (Mooney 1951; Tomar *et al.* 2016) to characterize the bulk viscosity,

$$\mu = \mu_f \exp\left(\frac{2.5\phi}{1 - k\phi}\right), \tag{2.18}$$

where μ_f, $\phi = c/\rho$ and k are the liquid viscosity at zero protein concentration, the volume fraction of protein in the bulk solution and the crowding factor ($1.35 < k < 1.91$), respectively.

To close the model, we need an additional equation for the gas pressure inside the bubble. In the first case study in which the bubble dissolves in a protein solution due to gas diffusion, we assume the temperature in the bubble T_g to remain constant and equal to the temperature in the bulk of the liquid, i.e. $T_g = T$. We let ϵ, ψ, V, n_g, M_g, m_g and D_ψ denote the Henry's constant with a unit kg m^{-3} Pa^{-1}, the gas concentration in the bulk of the liquid with a unit kg m^{-3}, the volume of the bubble, the amount of gas in the bubble with a unit mol, the molar weight of the gas, the mass of gas in the bubble, and the diffusion coefficient of the gas in the bulk of the liquid, respectively. The gas concentration in the liquid ψ is governed by (Epstein & Plesset 1950; Peñas-López *et al.* 2016)

$$\frac{\partial\psi}{\partial t} + v_r \frac{\partial\psi}{\partial r} = \frac{1}{r^2}\frac{\partial}{\partial r}\left(D_\psi r^2 \frac{\partial\psi}{\partial r}\right), \tag{2.19}$$

which is subject to

$$\psi|_{t=0} = \psi_\infty, \quad \psi|_{r\to\infty} = \psi_\infty, \quad \psi|_{t>0, r=R} = \epsilon p_g. \tag{2.20a–c}$$

The far-field gas concentration is $\psi_\infty = \epsilon(p_a - p_v)$, where p_a is the atmospheric pressure. The rate of change of the gas mass in the bubble is

$$\frac{\mathrm{d}m_g}{\mathrm{d}t} = 4\pi R^2 D_\psi \left.\frac{\partial\psi}{\partial r}\right|_{r=R}. \tag{2.21}$$

From the ideal gas law $p_g V = n_g R_g T_g$, we have

$$\frac{\mathrm{d}m_g}{\mathrm{d}t} = \frac{\mathrm{d}(n_g M_g)}{\mathrm{d}t} = \frac{\mathrm{d}}{\mathrm{d}t}\left(\frac{4\pi M_g R^3 p_g}{3R_g T_g}\right). \tag{2.22}$$

Coupling equations (2.21) and (2.22), we get

$$\frac{\mathrm{d}}{\mathrm{d}t}(p_g R^3) = 3D_\psi R^2 \frac{R_g T_g}{M_g}\frac{\partial \psi}{\partial r}\bigg|_{r=R}. \tag{2.23}$$

In the second case study in which an imposed fluctuating pressure drives the bubble to oscillate, we assume the gas pressure to follow a polytropic process,

$$p_g = p_{g0}\left(\frac{R_0}{R}\right)^{3\alpha}, \tag{2.24}$$

where p_{g0} and α are the gas pressure at $t = 0$ and the polytropic index, respectively; $\alpha = 1$ represents an isothermal process, and $\alpha = 1.4$ denotes an adiabatic process.

In the following two case studies, unless otherwise stated, we will use the values of the physical parameters listed in table 1. Bovine serum albumin (BSA) solution is considered here. Values for the varying surface tension of the solution–air interface and dynamic adsorption/desorption of protein are obtained by fitting to the experimental data from the literature (Fainerman *et al.* 1998; Ybert & di Meglio 1998; Miller *et al.* 2000). At $t = 0$, we assume that: (1) the velocity of the bubble surface $\dot{R}(t = 0) = 0$; (2) unless otherwise stated, the adsorption/desorption of protein is in equilibrium, i.e. $J = 0$, and thus the initial protein concentration at the bubble surface $\Gamma_0 = \theta^a c_\infty \Gamma_m/(\theta^a c_\infty + \theta^d)$; and (3) the initial gas pressure $p_{g0} = p_a - p_v + 2\gamma_0/R_0$, where γ_0 is the initial surface tension. We introduce $\zeta = 1 - 2R/r$ such that $r \in [R, \infty)$ maps to $\zeta \in [-1, 1)$. We let $\zeta = 0.98$, corresponding to $r = 100R$, represent the far field, and then we divide $\zeta \in [-1, 0.98]$ into 300 uniform intervals. We use the backward Euler method to solve (2.10), (2.13), (2.16), and (2.23) or (2.24).

3. Bubble dissolution in a protein solution

3.1. *Prediction of the dissolution rate*

The dissolution of a bubble is caused by the imbalanced gas concentration across the bubble surface. Initially, the surface excess stress is negligible because $\mathcal{F}(t = 0) = 0$. According to the Epstein–Plesset theory (Epstein & Plesset 1950), the surface velocity is

$$\frac{\mathrm{d}R}{\mathrm{d}t} = -\frac{R_g T D_\psi \epsilon}{p_g M_g}\frac{2\gamma}{R}\left(\frac{1}{R} + \frac{1}{\sqrt{\pi D_\psi t}}\right). \tag{3.1}$$

The above equation indicates that the dissolution rate increases with the gas diffusion coefficient but decreases with the bubble radius. Protein adsorption and desorption are in equilibrium at $t = 0$. If the protein concentration in the bulk solution c_∞ is low, increasing c_∞ consequently yields a higher protein concentration at the bubble surface, and hence a smaller surface tension. Thus at small t, the dissolution rate decreases with the protein

Density of protein solution	ρ	1000	kg m^{-3}
Protein concentration far from the bubble surface	c_∞	10	kg m^{-3}
Initial bubble radius	R_0	10^{-5}	m
Maximum protein concentration at the bubble surface	Γ_m	3×10^{-6}	kg m^{-2}
Crowding factor	k	1.5	—
Surface tension at zero protein concentration	γ_f	0.072	N m^{-1}
Minimum surface tension	γ_c	0.052	N m^{-1}
Fitting parameter in the equation of state for surface tension	Γ_p	3×10^{-6}	mol m^{-2}
Rate of change of dilatational elasticity with respect to protein concentration	E_{sl}	10^4	m^2 s^{-2}
Surface relaxation time	λ_s	1	s
Viscosity of protein solution at zero protein concentration	μ_f	10^{-3}	Pa s
Protein adsorption coefficient	θ^a	0.05	m^3 s^{-1} kg^{-1}
Protein desorption coefficient	θ^d	2×10^{-4}	s^{-1}
Atmospheric pressure	p_a	1.01×10^5	Pa
Vapour pressure	p_v	3010	Pa
Molar weight of air	M_g	0.02897	kg mol^{-1}
Gas constant	R_g	8.314	J mol^{-1} K^{-1}
Henry's constant of air	ϵ	1.74×10^{-7}	kg m^{-3} Pa^{-1}
Air diffusion coefficient in the protein solution	D_ψ	2×10^{-9}	m^2 s^{-1}
Protein diffusion coefficient in the bulk of the solution	D_c	10^{-11}	m^2 s^{-1}
Temperature in the protein solution	T	293.15	K
Polytropic index	α	1	—
Initial air density	ρ_{g0}	1.2	kg m^{-3}

Table 1. Physical parameters and their values.

concentration in the bulk of the liquid, as shown in figure 1. If we define $R = R_0\tilde{R}$ and $t = \lambda\tilde{t}$, where $\lambda = R_0^2/D_\psi$ is the gas diffusion time scale, then (3.1) can be rewritten as

$$\frac{\mathrm{d}\tilde{R}}{\mathrm{d}\tilde{t}} = -\frac{1}{We\,\tilde{R}}\left(\frac{1}{\tilde{R}} + \frac{1}{\sqrt{\pi\tilde{t}}}\right), \quad We = \frac{\rho_g/\epsilon}{2\gamma/R_0}, \tag{3.2a,b}$$

where ρ_g is the instantaneous gas density. The Weber number, We, compares the gas inertial force to the surface tension force. Thus, the surface tension drives the gas to leave the bubble (through diffusion), and the dissolution rate is initially determined by the ratio of the surface tension force to the gas inertial force. In other words, the dissolution of the bubble initially follows an inertio-capillary process. The dissolution rate decreases with the gas inertia, so, in medicine, where microbubbles are used to open cell membranes and deliver drugs, bubbles with a heavy gas core (e.g. C_3F_8 with density 8.17 kg m^{-3} or C_4F_{10} with density 11.2 kg m^{-3}) are generally used to extend the life of bubbles in the blood (Dauba *et al.* 2020).

We define Z_1 as the ratio of surface excess stress to the surface tension and Z_2 as the ratio of bulk viscous stress to the surface tension, i.e.

$$Z_1 = \left|\frac{4E_s\mathcal{F}}{R}\right| \Big/ \left(\frac{2\gamma}{R}\right) = \frac{2}{Ec}\int_0^t \exp[-(t-t')/\lambda_s]\frac{\dot{R}(t')}{R(t')}\,\mathrm{d}t', \tag{3.3}$$

$$Z_2 = \left|12R^2\dot{R}\int_R^\infty \frac{\mu(c)}{r^4}\,\mathrm{d}r\right| \Big/ \left(\frac{2\gamma}{R}\right) = \frac{3Ca}{4}\int_{-1}^1 \exp\left(\frac{2.5\phi}{1-k\phi}\right)(1-\zeta)^2\,\mathrm{d}\zeta. \tag{3.4}$$

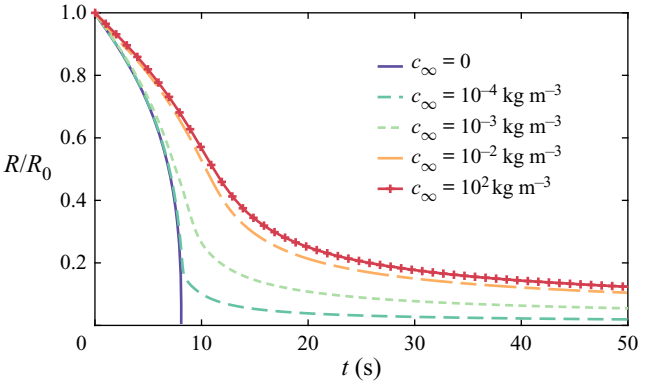

Figure 1. Effect of protein concentration on the bubble dissolution process.

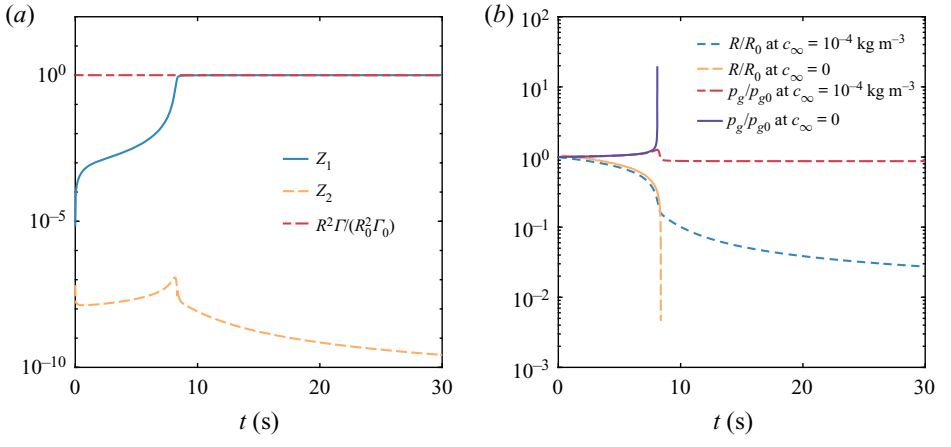

Figure 2. (*a*) Time evolution of the total protein on the bubble surface ΓR^2, the ratio of surface excess stress to the surface tension Z_1, and the ratio of bulk viscous stress to the surface tension Z_2 in the case of $c_\infty = 10^{-4}$ kg m^{-3}. (*b*) Comparison of the bubble behaviour in water and in a protein solution with $c_\infty = 10^{-4}$ kg m^{-3}.

Here $Ec = \gamma/E_s$ is the elasto-capillary number, which compares the surface tension and surface dilatational elasticity; and $Ca = \mu_f \dot{R}/\gamma$ is the capillary number, which measures the importance of the viscous stress in the bulk of the liquid compared to the surface tension.

As the bubble shrinks, the protein density at the bubble surface increases, which leads to the growth of the surface excess stress, as shown in figure 2(*a*). The rate of dissolution is determined by the gas inertial force, surface tension force and surface excess stress, during which the dissolution of the bubble follows an inertio-elasto-capillary process. As the bubble progressively shrinks, the surface excess stress eventually balances the surface tension force, and the dissolution of the bubble follows an elasto-capillary process.

For a Newtonian interface (i.e. the surface relaxation time goes to zero), the balance of surface tension force and surface dilatational viscous stress yields $\dot{R} = -\gamma R/(2\kappa_s)$. Thus, the dissolution rate for a bubble with a Newtonian interface (e.g. a surfactant- or lipid-coated bubble) is inversely proportional to the surface dilatational viscosity.

For an elastic interface (i.e. the surface relaxation time goes to infinity), the balance of surface tension force and surface dilatational elastic stress yields $R/R_0 = \exp[-\gamma/(2E_s)] = \exp[-Ec/2]$. Thus the dimensionless bubble radius is solely determined by the elasto-capillary number. A value $Z_2 \ll 1$ also indicates that the viscous stress in the bulk of the liquid is negligible. Additionally, after the surface excess stress balances the surface tension force, the bubble dissolution rate is small such that the gas pressure inside the bubble p_g remains almost constant (close to atmospheric pressure), as shown in figure 2(*b*).

Next, we aim to obtain the dissolution rate of a protein-coated bubble after the surface excess stress balances the surface tension, i.e. $Z_1 = 1$. Let us consider a protein solution with high concentration that satisfies $\theta^a c_\infty \gg \theta^d$; then $\Gamma_0 = \theta^a c_\infty \Gamma_m/(\theta^a c_\infty + \theta^d) \approx \Gamma_m$, which is the maximum packing density of proteins at the bubble surface. Proteins typically have a low desorption ability. Thus, the protein concentration at the bubble surface increases as the bubble shrinks, i.e. $\Gamma(t) \geq \Gamma_m$, which yields $\gamma = \gamma_c$ (i.e. the surface tension remains constant as the bubble shrinks) and $J = -\theta^d \Gamma$. Using (2.16), we obtain the total protein at the bubble surface $\Gamma R^2 = \Gamma_0 R_0^2 \exp(-\theta^d t)$, which decreases exponentially with time, and the decay rate equals the protein desorption constant. Substituting the expression of Γ into $Z_1 = 1$, i.e. the balance of surface tension and surface excess stress, we get

$$\mathcal{F} = -\frac{\gamma_c}{2E_s} = -\frac{\gamma_c}{2E_{sl}\Gamma} = -\frac{\gamma_c R^2 \exp(\theta^d t)}{2E_{sl}\Gamma_0 R_0^2}. \tag{3.5}$$

Substituting (3.5) into $\dot{\mathcal{F}} + \mathcal{F}/\lambda_s = \dot{R}/R$ and after some manipulations, we obtain

$$\frac{\mathrm{d}R}{\mathrm{d}t} = -\frac{R_0}{2\lambda_s} \frac{(\theta^d \lambda_s + 1)(R/R_0)^3}{(R/R_0)^2 + \exp(-\theta^d t)/Ec_0}, \tag{3.6}$$

where $Ec_0 = \gamma_c/(E_{sl}\Gamma_0) = \gamma_c/E_{s0}$ denotes the ratio of the surface tension to the initial surface dilatational elasticity, E_{s0}.

The dissolution rate will not reduce to zero (i.e. the bubble will not remain static) because (1) the surface excess stress relaxes (decreases) when the strain on the surface remains constant and (2) protein desorbs from the bubble surface, which reduces the surface excess stress. If $\theta^d \lambda_s \ll 1$, the variation of the surface excess stress with respect to time is mainly caused by the surface relaxation, and the dissolution rate is inversely proportional to the surface relaxation time λ_s at large t, as indicated by (3.6). If $\theta^d \lambda_s \gg 1$, the variation of the surface excess stress is induced by the protein desorption from the bubble surface, and hence the dissolution rate is independent of the surface relaxation time λ_s. Verification of the Epstein–Plesset theory (short-time asymptotic), i.e. (3.1), and the long-time asymptotic, i.e. (3.6), are shown in figure 3.

During the elasto-capillary process, let us use the surface relaxation time λ_s as the time scale and define $t = \lambda_s \check{t}$. Then (3.6) can be rewritten as

$$\frac{\mathrm{d}\tilde{R}}{\mathrm{d}\check{t}} = -\frac{(\theta^d \lambda_s + 1)\tilde{R}^3}{2(\exp(-\theta^d \lambda_s \check{t})/Ec_0 + \tilde{R}^2)}. \tag{3.7}$$

In the limiting case of $\theta^d \lambda_s \check{t} \ll 1$ or $\theta^d \lambda_s \check{t} \gg 1$, (3.7) reduces to

$$\frac{\mathrm{d}\tilde{R}}{\mathrm{d}\check{t}} = \begin{cases} -(\theta^d \lambda_s + 1)\tilde{R}^3/[2(Ec_0^{-1} + \tilde{R}^2)], & \text{when } \theta^d \lambda_s \check{t} \ll 1, \\ -(\theta^d \lambda_s + 1)\tilde{R}/2, & \text{when } \theta^d \lambda_s \check{t} \gg 1. \end{cases} \tag{3.8}$$

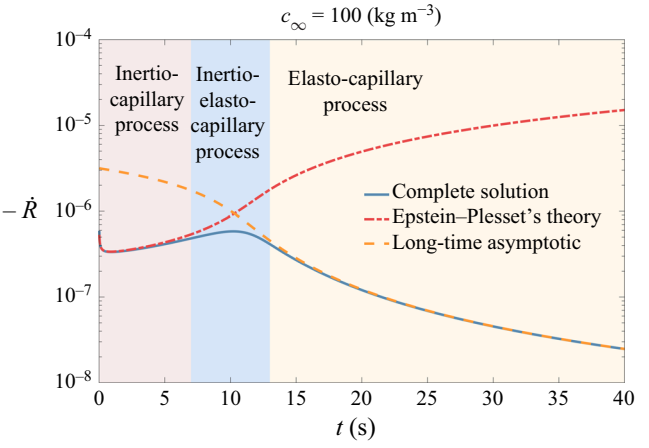

Figure 3. The time evolution of the dissolution rate.

The continuous decrease of $\tilde{R}$ yields a progressive reduction of the dissolution rate on both short and long time scales ($\theta^d \lambda_s \check{t}$ is much less or much greater than one). As the bubble shrinks, on the one hand, the reduction of the surface area increases the protein density on the bubble surface (i.e. decelerates dissolution); on the other hand, the protein desorbs from the bubble, which reduces the protein density on the bubble surface (i.e. accelerates dissolution). Thus, the bubble may accelerate or decelerate shrinking at intermediate scale ($\theta^d \lambda_s \check{t}$ of the order of one), depending on the magnitude of protein desorption ability and surface dilatational elasticity, as indicated by (3.7). Additionally, the surface relaxation time and surface dilatational elasticity help stabilize the bubble against dissolution, as shown in figure 4.

Khan & Dalvi (2020) performed experiments to study the dissolution behaviour of microbubbles in aqueous BSA solution (3 % w/v). They observed that: (1) the protein-coated bubble shrinks at a slow rate (compared to the uncoated bubble) before the bubble buckles; and (2) once the bubble buckles, a large portion of the protein detaches from the bubble surface, and the microbubble quickly disappears. This is different from the behaviour of lipid-coated bubbles, which stay for a while after buckling because the surface tension also reduces to zero (Marmottant *et al.* 2005). Our model well captures the kinetics of the BSA-coated bubble before it buckles, as shown in figure 5. Additionally, a larger BSA-coated bubble has a longer relaxation time according to our calibration results. An uncoated microbubble can only stay in water for approximately 1 s, but the time for a protein-coated microbubble to disappear after buckling is of the order of 10 s (Khan & Dalvi 2020). Two reasons may explain this: (1) the bubble is non-spherical after buckling; and/or (2) there is a small amount of protein left on the bubble surface; thus, the protein structure provides resistance.

3.2. *Protein adsorption to an initially clean bubble surface*

The protein adsorption to a bubble surface consists of two steps: (1) proteins in the bulk solution advect/diffuse to the adjacent layer of the bubble surface; and (2) proteins in the adjacent layer adsorb to the bubble surface (Manikantan & Squires 2020). For a static spherical bubble with a kinetic-limited flux (i.e. $c|_{r=R} = c_\infty$), the rate of change of the

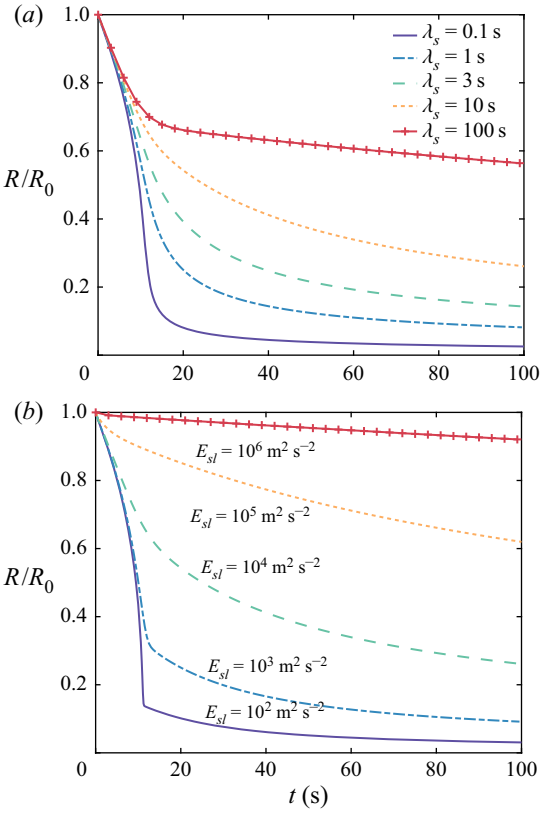

Figure 4. (*a*) Effects of surface relaxation time on the bubble dynamics; $E_{sl} = 10^4$ m^2 s^{-2} is used here. (*b*) Effects of surface dilatational elasticity on the bubble dynamics; $\lambda_s = 10$ s is used here.

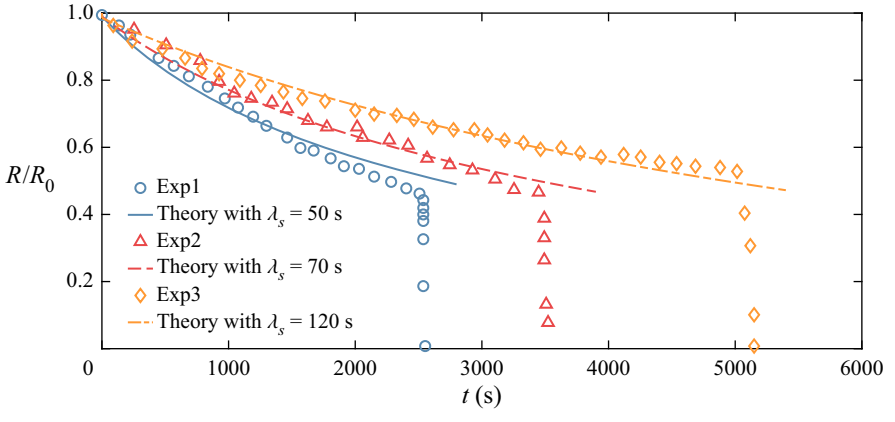

Figure 5. Comparison between our model predictions and experimental data for the dissolution of microbubbles in aqueous BSA solution (3 % w/v) (Khan & Dalvi 2020). All experiments were performed at room temperature. The BSA solution was preheated up to 70 ± 1 °C to produce a stable BSA microbubble formulation (Khan & Dalvi 2020). Symbols: ○, experimental data with initial bubble diameter 6.9 μm; △, experimental data with initial bubble diameter 10.8 μm; ◇, experimental data with initial bubble diameter 14.7 μm. Here $E_{sl} = 4 \times 10^5$ m^2 s^{-2} is used in these three model predictions.

protein concentration on the bubble surface is governed by

$$\frac{\mathrm{d}\Gamma}{\mathrm{d}t} = \theta^a c_\infty \Gamma_m - (\theta^a c_\infty + \theta^d)\Gamma, \tag{3.9}$$

which yields a characteristic time scale, $\tau_k = 1/(\theta^a c_\infty + \theta^d)$, for kinetic-limited adsorption (Jin, Balasubramaniam & Stebe 2004). For a static spherical bubble with diffusion-limited adsorption, the protein adsorption/desorption on the bubble surface is rapid such that the protein concentration on the bubble surface satisfies the adsorption isotherm.

The mass of proteins on the bubble can be estimated by $4\pi R^2 \Gamma_{eq}$, where $\Gamma_{eq} = \theta^a c_\infty \Gamma_m/(\theta^a c_\infty + \theta^d)$. Assuming that there is a thin layer (around the bubble surface) in the bulk solution supplying proteins to the surface, i.e.

$$4\pi R^2 \Gamma_{eq} = \frac{4}{3}\pi c_\infty [(R + h_s)^3 - R^3], \tag{3.10}$$

we obtain the thickness of this thin layer (Alvarez, Walker & Anna 2010*b*,*a*) as

$$h_s = R\left[\left(\frac{3h_p}{R} + 1\right)^{1/3} - 1\right]. \tag{3.11}$$

Here h_s is called the intrinsic spherical depletion depth; and $h_p = \Gamma_{eq}/c_\infty$ is the intrinsic planar depletion depth (Jin *et al.* 2004; Alvarez *et al.* 2010*a*).

The flux boundary condition

$$\frac{\mathrm{d}\Gamma}{\mathrm{d}t} = D_c \frac{\partial c}{\partial r}\bigg|_{r=R} \tag{3.12}$$

has a characteristic time scale $\tau_{D1} = h_s h_p/D_c$, derived from $\Gamma_{eq}/\tau_{D1} \sim D_c c_\infty/h_s$. The diffusion equation (2.13) for proteins in the bulk solution has another characteristic time scale $\tau_{D2} = h_s^2/D_c$, derived from $c_\infty/\tau_{D2} \sim D_c c_\infty/h_s^2$. Alvarez *et al.* (2010*a*) used

$$\tau_D = (\tau_{D1}\tau_{D2})^{1/2} = \frac{(h_s^3 h_p)^{1/2}}{D_c} \tag{3.13}$$

to represent the characteristic time scale for diffusion-limited adsorption and validated this time scale in experiments (Alvarez *et al.* 2010*b*).

If the bubble radius is much smaller than the intrinsic planar depletion depth, i.e. $R \ll h_p$, then

$$\tau_D = \frac{\sqrt{3}\, h_p R}{D_c} = \frac{\sqrt{3}\,\theta^a \Gamma_m}{\theta^a c_\infty + \theta^d}\frac{R}{D_c} = \tau_k\left(\frac{\sqrt{3}\,\theta^a R \Gamma_m}{D_c}\right). \tag{3.14}$$

For a small bubble ($R \ll h_p$), the characteristic time scale of the diffusion-limited adsorption is proportional to the bubble radius and inversely proportional to the protein diffusion coefficient in the bulk solution. If the bubble radius is much greater than the intrinsic spherical depletion depth, i.e. $R \gg h_p$, the spherical depletion depth approaches the planar depletion depth, and the characteristic time scale for the diffusion-limited adsorption is

$$\tau_D = \frac{h_p^2}{D_c} = \frac{1}{D_c}\left(\frac{\theta^a \Gamma_m}{\theta^a c_\infty + \theta^d}\right)^2 = \tau_k\left[\frac{(\theta^a \Gamma_m)^2}{D_c(\theta^a c_\infty + \theta^d)}\right]. \tag{3.15}$$

Thus, the diffusion time scale is inversely proportional to the protein diffusion coefficient in the bulk solution but independent of the bubble radius when $R \gg h_p$.

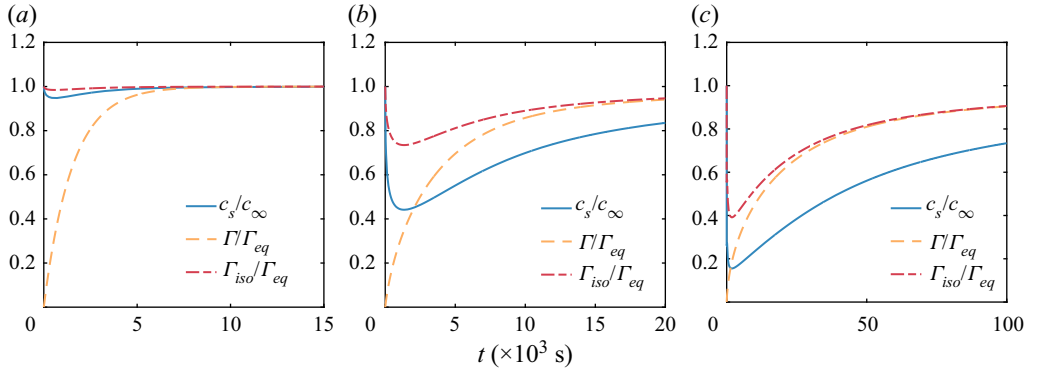

Figure 6. Protein adsorption to a large bubble for: (*a*) $D_c = 10^{-9}$ m^2 s^{-1}, $\tau_D = 35$ s; (*b*) $D_c = 10^{-11}$ m^2 s^{-1}, $\tau_D = 3500$ s; and (*c*) $D_c = 10^{-12}$ m^2 s^{-1}, $\tau_D = 35\,000$ s. Here $R_0 = 1$ mm and $c_\infty = 0.01$ kg m^{-3} are used; and $\tau_{dis1} = 5 \times 10^{12}$ s and $\tau_{dis2} = 5 \times 10^7$ s are much larger than τ_D and $\tau_k = 1400$ s such that the bubble radius remains almost constant.

If a clean bubble is formed in a protein solution, i.e. $\Gamma(t = 0) = 0$, proteins adsorb to the bubble's surface while the bubble shrinks simultaneously. Before the surface excess stress becomes significant, the dimensionless dissolution rate is governed by (3.2*a*,*b*). When $\tilde{t} \ll 1$, $\mathrm{d}\tilde{R}/\mathrm{d}\tilde{t} \sim 1/(We\,\tilde{R}\sqrt{\pi\tilde{t}})$ yields a dimensionless time scale $\tilde{\tau}_{dis1} = We^2$, and hence the dimensional time scale is

$$\tau_{dis1} = \lambda\tilde{\tau}_{dis1} \sim \frac{\rho_{g0}^2 R_0^4}{\epsilon^2\gamma_f^2 D_\psi}, \tag{3.16}$$

where ρ_{g0} is the initial gas density. When $\tilde{t} \gg 1$, $\mathrm{d}\tilde{R}/\mathrm{d}\tilde{t} \sim 1/(We\,\tilde{R}^2)$ yields another dimensionless time scale $\tilde{\tau}_{dis2} = We$, and hence the dimensional time scale is

$$\tau_{dis2} = \lambda\tilde{\tau}_{dis2} \sim \frac{\rho_{g0} R_0^3}{\epsilon\gamma_f D_\psi}. \tag{3.17}$$

Thus, the characteristic time scale τ_{dis} for the bubble dissolution is inversely proportional to the gas diffusion coefficient. Additionally, τ_{dis} follows R_0^4 when $t \ll R_0^2/D_\psi$; as t grows, τ_{dis} follows R_0^3 until the surface excess stress becomes significant.

The small bubble quickly dissolves in the protein solution (τ_{dis} is much less than τ_D and τ_k), and hence proteins have no time to adsorb to the bubble surface. For a large bubble, τ_{dis} is much greater than τ_D and τ_k such that the bubble can be treated as static. Figure 6 shows the protein adsorption to a large (static) bubble in three different cases: $\tau_D \ll \tau_k$, $\tau_D \sim \tau_k$ and $\tau_D \gg \tau_k$. In the case of kinetic-limited adsorption ($\tau_D \ll \tau_k$), $c_s \approx c_\infty$ and the protein adsorption rate on the bubble is constrained by the protein adsorption/desorption ability (θ^a and θ^d), as shown in figure 6(*a*). In the case of diffusion-limited adsorption, i.e. $\tau_D \gg \tau_k$, the protein adsorption rate on the bubble is constrained by c_s (i.e. the protein diffusion coefficient D_c), and $\Gamma \approx \Gamma_{iso} = \theta^a c_s \Gamma_m/(\theta^a c_s + \theta^d)$, as shown in figure 6(*c*).

Figure 7 shows the transition from diffusion-limited to kinetic-limited behaviour as the bubble shrinks. If we use $R_0 = 0.2$ mm, $D_c = 10^{-12}$ m^2 s^{-1}, $\theta^a = 0.05$ m^3 (s kg)$^{-1}$ and $\theta^d = 0.0002$ s^{-1}, then $\tau_D = 20\,000$ s and $\tau_k = 1400$ s. The protein adsorption initially is diffusion-limited, and increasing the protein diffusion coefficient D_c effectively improves the protein adsorption rate. The protein concentration on the bubble surface Γ grows with

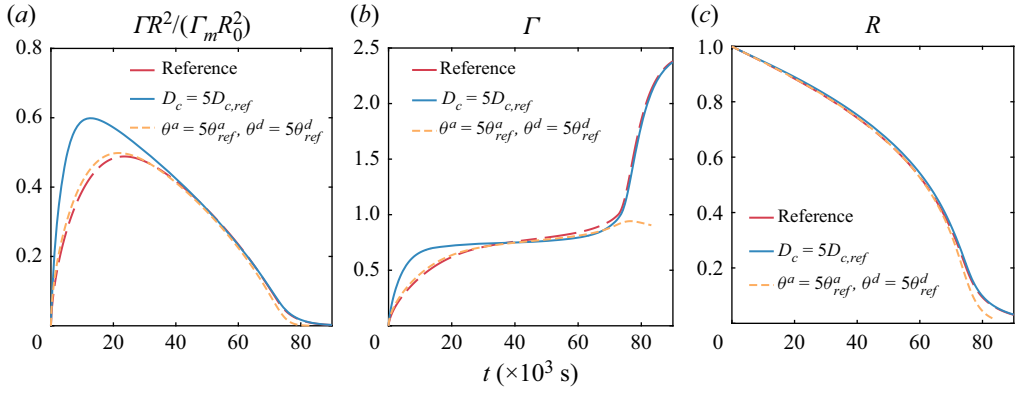

Figure 7. Transition from the diffusion-limited to the kinetic-limited behaviour. Here we use $R_0 = 0.2$ mm, $c_\infty = 0.01$ kg m^{-3}, $E_{sl} = 7 \times 10^5$ m^2 s^{-2} and $\lambda_s = 50$ s. The red dash-dotted line is used as the reference: $D_c = D_{c,ref} = 10^{-12}$ m^2 s^{-1}, $\theta^a = \theta^a_{ref} = 0.05$ m^3 (s kg)$^{-1}$ and $\theta^d = \theta^d_{ref} = 0.0002$ s^{-1}. Blue solid line: $D_c = 5D_{c,ref}$, $\theta^a = \theta^a_{ref}$ and $\theta^d = \theta^d_{ref}$. Orange dashed line: $D_c = D_{c,ref}$, $\theta^a = 5\theta^a_{ref}$ and $\theta^d = 5\theta^d_{ref}$.

the adsorption of proteins and the reduction of the surface area. When Γ exceeds Γ_m, the net flux of proteins to the interface is constrained by the protein desorption ability ($J = -\theta^d \Gamma$); in other words, the protein diffusion coefficient D_c no longer influences the bubble behaviour and the protein concentration on the bubble.

The reduction of surface area increases the protein concentration on the bubble Γ, but proteins desorb from the bubble simultaneously. Therefore, after Γ increases to Γ_{eq}, the value (trend) of Γ depends on the magnitude of the bubble dissolution rate, the protein diffusion coefficient in the bulk solution and the protein adsorption/desorption ability:

(i) If the bubble dissolution rate is much less than the protein desorption rate and the protein diffusion rate in the bulk solution, the protein concentration on the bubble surface Γ remains at equilibrium as the bubble shrinks, i.e. $\Gamma = \Gamma_{eq} = \theta^a c_\infty/(\theta^a c_\infty + \theta^d)$.

(ii) If the protein diffusion rate in the bulk solution is much lower than the bubble dissolution rate, and also the dissolution rate is much less than the protein desorption rate, then in that case proteins in the bulk solution around the bubble surface will accumulate such that $c_s \gg c_\infty$ and $\Gamma = \Gamma_m$.

(iii) If the protein desorption rate is much lower than the bubble dissolution rate, then the mass of proteins on the bubble ΓR^2 remains almost constant.

The bubble dissolution rate depends on the surface rheology, as discussed in § 3.1. The effects of the surface rheology on the protein adsorption/desorption rate are shown in figure 8.

The interfacial parameters, even for BSA, depending on the experimental procedures, can vary by orders of magnitude. Thus, identifying interfacial parameters that have significant effects on the protein adsorption rate helps the design of experiments. Table 2 summarizes the bubble dynamics and the corresponding important interfacial parameters in different scenarios. Before the protein concentration on the bubble Γ reaches Γ_{eq}, Γ grows as the bubble shrinks due to the adsorption of proteins and the reduction of surface area. The rate of protein adsorption depends on the protein adsorption/desorption ability, protein diffusion coefficient and the bubble dissolution rate. Before the surface excess stress becomes significant and balances the surface tension force, the bubble dissolution

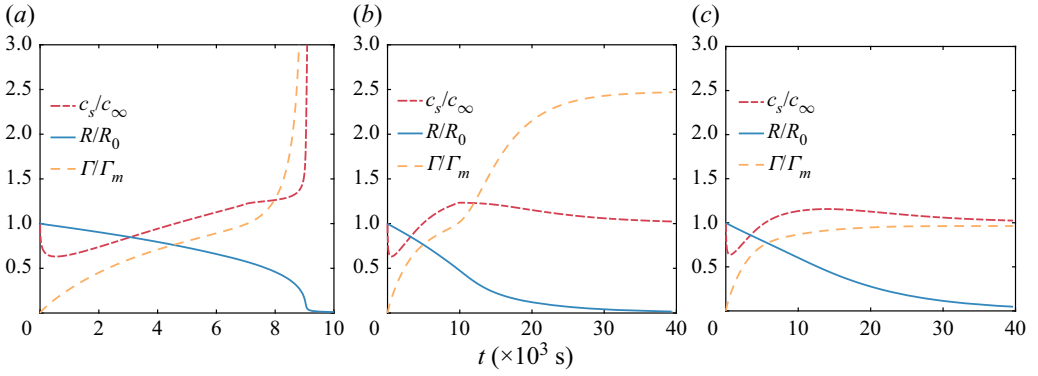

Figure 8. Effects of the surface rheology on the protein adsorption/desorption rate for: (*a*) $E_{sl} = 10^4$ m^2 s^{-2}, $\lambda_s = 1$ s; (*b*) $E_{sl} = 7 \times 10^5$ m^2 s^{-2}, $\lambda_s = 50$ s; and (*c*) $E_{sl} = 10^6$ m^2 s^{-2}, $\lambda_s = 100$ s. Here $R_0 = 0.1$ mm, $c_\infty = 0.01$ kg m^{-3} and $D_c = 10^{-11}$ m^2 s^{-1} are used; and $\tau_k = 1400$ s, $\tau_D = 6600$ s, $\tau_{dis1} = 5 \times 10^8$ s and $\tau_{dis2} = 5 \times 10^4$ s.

Regimes	Characteristics	Important interfacial parameters
$\tau_{dis} \ll \tau_D$ or $\tau_{dis} \ll \tau_k$	Bubble quickly dissolves with no proteins on it	γ
$\tau_k \ll \tau_D \ll \tau_{dis}$	Static bubble with diffusion-limited adsorption	D_c
$\tau_D \ll \tau_k \ll \tau_{dis}$	Static bubble with kinetic-limited adsorption	θ^a, θ^d
$\tau_D \sim \tau_k$ and $\tau_D \ll \tau_{dis}$	Static bubble with kinetic-diffusion-controlled adsorption	D_c, θ^a, θ^d
$\tau_{dis} \sim \tau_D$ and $\tau_k \ll \tau_D$	Transition from diffusion-limited to kinetic-limited behaviour	D_c, θ^a, θ^d, γ, E_{sl}, λ_s
$\tau_{dis} \sim \tau_k$ and $\tau_D \ll \tau_k$	Kinetic-limited transport	θ^a, θ^d, γ, E_{sl}, λ_s
$\tau_{dis} \sim \tau_k \sim \tau_D$	Kinetic-diffusion-controlled transport	D_c, θ^a, θ^d, γ, E_{sl}, λ_s

Table 2. The bubble dynamics and the corresponding important interfacial parameters.

rate depends on the gas density, gas diffusion coefficient and surface tension. However, after the surface excess stress balances the surface tension force, the surface dilatational elasticity E_s and the surface relaxation time λ_s become important, and the gas properties become insignificant. If the protein concentration on the bubble grows beyond Γ_{eq} but smaller than Γ_m, the protein concentration on the bubble is still affected by the protein diffusion coefficient, protein adsorption/desorption ability and the bubble dissolution rate. Once the protein concentration on the bubble exceeds Γ_m, the net flux of proteins to the bubble only depends on the protein desorption ability θ^d; therefore, the protein adsorption ability θ^a and the protein diffusion coefficient D_c become unimportant.

4. Response of a protein-coated bubble to an imposed fluctuating pressure

In this case, we consider a protein-coated bubble oscillating in a pressure field $p_\infty = p_a[1 + \varepsilon \cos(\omega t)]$. Let us consider a small fluctuating pressure ($\varepsilon \ll 1$), that the system is linear, and hence the bubble responds at the driving frequency at the steady state

(Brennen 2013). To simplify this problem, we will neglect gas diffusion. We also ignore the adsorption/desorption of protein since its time scale (of the order of seconds) generally is much greater than the period of imposed pressure (of the order of microseconds or milliseconds). Additionally, we ignore the variation of the protein concentration in the bulk of the liquid such that the bulk viscosity μ is independent of radial position r.

Let subscript E denote the equilibrium state. We write the complex form of the pressure at infinity as $p_\infty = p_a + \varepsilon p_a e^{j\omega t}$, where $j = \sqrt{-1}$; then its physical form (projection onto the real axis) is $p_\infty = p_a + \mathrm{Re}\{\varepsilon p_a e^{j\omega t}\}$. Similarly, we express the complex form of the bubble radius R, protein concentration at the bubble surface Γ, gas pressure inside the bubble p_g and surface tension γ as

$$R = R_E(1+\hat{R}e^{j\omega t}),\quad \Gamma = \Gamma_E(1+\hat{\Gamma}e^{j\omega t}),\quad p_g = p_{gE}(1+\hat{p}_g e^{j\omega t}),\quad \gamma = \gamma_E(1+\hat{\gamma}e^{j\omega t}). \tag{4.1a–d}$$

Substituting them into (2.16), (2.17) and (2.24) and then linearizing, we get $\hat{\Gamma} = -2\hat{R}$, $\hat{p}_g = -3\alpha\hat{R}$ and $\hat{\gamma} = \chi\hat{R}$, where

$$\chi = \begin{cases} \left(\dfrac{R_g T \Gamma_p}{\gamma_E}\right)\left(\dfrac{2\Gamma_E}{\Gamma_m - \Gamma_E}\right), & \text{when } \Gamma_E \le \Gamma_c, \\ 0, & \text{when } \Gamma_E > \Gamma_c. \end{cases} \tag{4.2}$$

We assume $\mathcal{F} = \mathcal{F}_E + \hat{\mathcal{F}}e^{j\omega t}$ and substitute it into $\dot{\mathcal{F}} + \mathcal{F}/\lambda_s = \dot{R}/R$. After linearization we obtain $\mathcal{F}_E = 0$ and $\hat{\mathcal{F}} = (j\omega\lambda_s + \omega^2\lambda_s^2)\hat{R}/(1+\omega^2\lambda_s^2)$, and thus the surface excess stress is zero at the equilibrium state. Substituting the expressions of p_∞, R, Γ, γ and $\mathcal{F}$ into (2.9) and linearizing, we get the zeroth-order solution

$$p_v + p_{gE} - p_a - 2\gamma_E/R_E = 0, \tag{4.3}$$

and the first-order solution

$$\frac{\varepsilon p_a}{\rho R_E^2 \hat{R}} = \omega^2 - \frac{4j\omega}{\rho R_E^2}\left[\mu + \frac{\kappa_{sE}}{R_E}\frac{1}{1+(\omega\lambda_s)^2}\right] - \frac{1}{\rho R_E^2}\left[3\alpha(p_a - p_v) + \frac{2\gamma_E}{R_E}(\chi + 3\alpha - 1) + \frac{4E_{sE}}{R_E}\frac{(\omega\lambda_s)^2}{1+(\omega\lambda_s)^2}\right], \tag{4.4}$$

where $\kappa_{sE} = \kappa_{sl}\Gamma_E$ and $E_{sE} = E_{sl}\Gamma_E$ are the surface dilatational viscosity and dilatational elasticity at the equilibrium state, respectively.

Equation (4.4) is a solution of a forced oscillation, in which a mass $m = \rho R_E^3$, attached to a spring and a dashpot in parallel arrangement, oscillates under an external force $F_e = \varepsilon p_a R_E^2 \cos(\omega t)$, as shown in figure 9. The stiffness of the spring, s, and the resistance from the dashpot, R_m, are

$$s = m\omega_0^2 + 2\chi\gamma_E + 4E_{sE}\frac{(\omega\lambda_s)^2}{1+(\omega\lambda_s)^2}, \tag{4.5}$$

$$R_m = 2m\beta_0 + \frac{4\kappa_{sE}}{1+(\omega\lambda_s)^2}, \tag{4.6}$$

where $\omega_0 = \{[3\alpha(p_a - p_v)R_E + 2\gamma_E(3\alpha - 1)]/(\rho R_E^3)\}^{1/2}$ and $\beta_0 = 2\mu/(\rho R_E^2)$ are the natural frequency and the damping coefficient of the uncoated bubble, respectively.

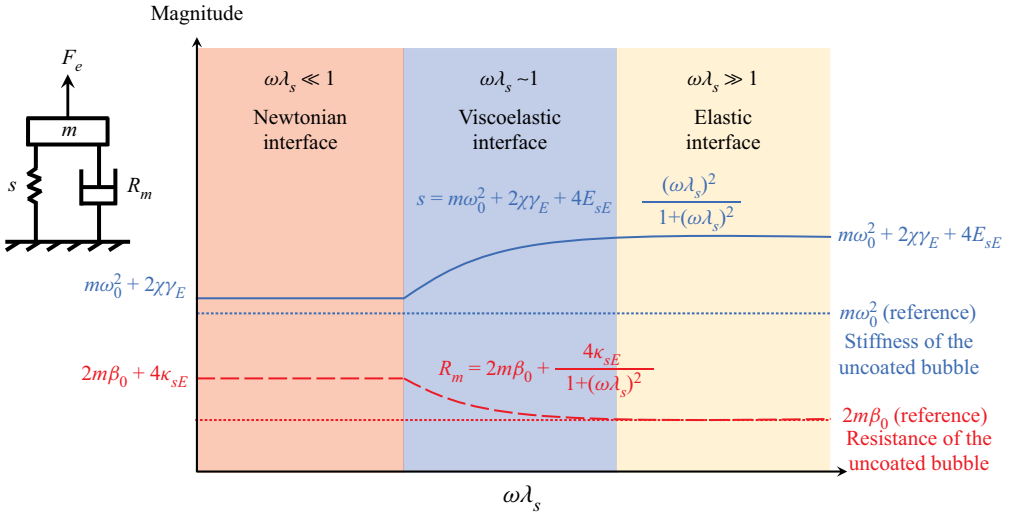

Figure 9. Effects of surface dilatational viscosity and dilatational elasticity on the resistance and stiffness of the system. Here ω_0 and β_0 are the natural frequency and damping coefficient of an uncoated bubble, respectively.

The restoring force provided by the viscoelastic bubble surface includes an elastic force (due to the surface dilatational elasticity) and a viscous force (due to the surface dilatational viscosity). The surface dilatational viscosity contributes to the resistance term, $4\kappa_{sE}/(1+\omega^2\lambda_s^2)$, which decreases with $\omega\lambda_s$. The surface dilatational elasticity contributes to the stiffness term, $4E_{sE}\omega^2\lambda_s^2/(1+\omega^2\lambda_s^2)$, which increases with $\omega\lambda_s$. Additionally, the variation of surface tension with protein concentration at the bubble surface, χ, adds additional stiffness to the system, which is independent of the acoustic frequency.

Let $\beta = R_m/(2m)$ and $\omega_n = \sqrt{s/m}$ denote the damping coefficient and the natural frequency, respectively. The amplitude of the dimensionless bubble radius is

$$\Lambda = |\hat{R}| = \frac{\varepsilon p_a}{\rho R_E^2 \sqrt{4\beta^2\omega^2 + (\omega_n^2 - \omega^2)^2}}. \tag{4.7}$$

We find a critical frequency

$$\omega_c = \sqrt{\omega_0^2 + \frac{2}{\rho R_E^2}\left(\frac{\chi\gamma_E}{R_E} + \frac{E_{sE}}{R_E} + \frac{2\mu}{\lambda_s}\right)}, \tag{4.8}$$

at which the viscoelasticity of the bubble surface does not affect the amplitude of oscillation: $\Lambda(\kappa_{sE}, E_{sE}) \geq \Lambda(\kappa_{sE} = 0, E_{sE} = 0)$ if $\omega \geq \omega_c$, otherwise $\Lambda(\kappa_{sE}, E_{sE}) < \Lambda(\kappa_{sE} = 0, E_{sE} = 0)$. Thus, for a Newtonian interface (surface relaxation time λ_s approaches zero and hence the critical frequency ω_c becomes infinitely large), including the surface dilatational viscosity reduces the oscillation amplitude. For a viscoelastic bubble surface, viscoelasticity enlarges the oscillation amplitude if and only if $\omega > \omega_c$ (i.e. the imposed acoustic pressure has a high frequency). We define $\mathcal{A} \equiv \Lambda/\Lambda_0$, where Λ_0 is the amplitude of the bubble radius at zero surface dilatational elasticity and dilatational viscosity. The effects of surface dilatational elasticity and dilatational viscosity on the dimensionless amplitude $\mathcal{A}$ are shown in figure 10.

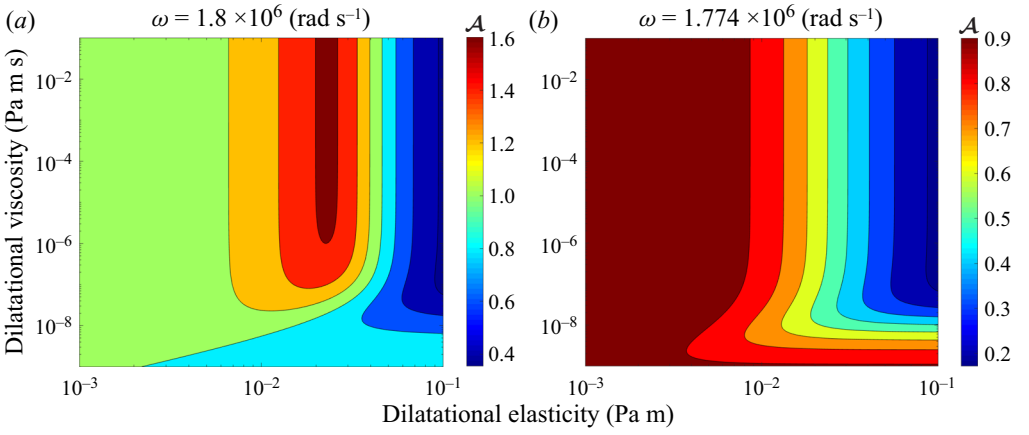

Figure 10. Effects of surface dilatational viscosity and surface dilatational elasticity on the amplitude of the dimensionless bubble radius $\mathcal{A}$. Here $R_E = 10^{-5}$ m, $\mu = 0.001$ Pa s, $\gamma_E = 0.052$ N m^{-1} and $\chi = 0$ are used. The natural frequency of the uncoated bubble is $\omega_0 = 1.774 \times 10^6$rad s^{-1}. (*a*) The frequency of the acoustic pressure is $\omega = 1.8 \times 10^6$ rad s^{-1}, which is slightly larger than ω_0; and (*b*) here $\omega = \omega_0$.

The resonant frequency, ω_r, and the maximum amplitude of the dimensionless bubble radius, $\Lambda_{max} = |\hat{R}|_{max}$, satisfy

$$\omega_r^2 = \omega_n^2 - 2\beta^2, \quad \Lambda_{max} = \left(\frac{\varepsilon p_a}{\rho R_E^2}\right)\left(\frac{1}{2\beta\sqrt{\omega_n^2 - \beta^2}}\right). \tag{4.9a,b}$$

The natural frequency ω_n and the damping coefficient β vary with the frequency of the imposed pressure ω; thus we need to solve $\omega_r^2 = \omega_n^2 - 2\beta^2$ numerically to obtain the resonant frequency ω_r. However, the explicit resonance frequency can be obtained in the following two limiting cases: (1) if $\omega\lambda_s \ll 1$, the bubble surface is Newtonian and hence it only contributes resistance, the natural frequency is $\omega_n = \{\omega_0^2 + 2\chi\gamma_E/m\}^{1/2}$ and the damping coefficient of the bubble is $\beta = \beta_0 + 2\kappa_{sE}/m$; and (2) if $\omega\lambda_s \gg 1$, the bubble surface is purely elastic, which only contributes stiffness, then the natural frequency is $\omega_n = \{\omega_0^2 + (2\chi\gamma_E + 4E_{sE})/m\}^{1/2}$ and the damping coefficient of the bubble is $\beta = \beta_0$. The effects of surface dilatational viscosity and surface dilatational elasticity on the resonant amplitude and frequency are shown in figure 11.

If we want to measure the dilatational elasticity and the relaxation time of the viscoelastic bubble surface, we can consider performing two experiments: (1) Impose a small fluctuating pressure with a frequency near the natural frequency of the uncoated bubble. In this case, $\omega\lambda_s$ generally is much greater than one, and hence the amplitude of oscillation is independent of the relaxation time; thus, we can use (4.7) to determine the surface dilatational elasticity. (2) After obtaining the surface dilatational elasticity, we can adjust the frequency to around $1/\lambda_s$ (generally in the range of 0.001–1 s^{-1}) and get the corresponding oscillation amplitude; next, we use (4.7) to determine the relaxation time. However, in the second experiment with a low frequency, we need to minimize the effect of gas diffusion on the bubble dynamics (e.g. we can do experiments in a saturated solution (Epstein & Plesset 1950) or use gas that has a low diffusion coefficient in the liquid). Additionally, if the ratio of the surface dilatational elasticity to the equilibrium bubble radius, E_{sE}/R_E, is much less than atmospheric pressure or the surface tension $2\gamma_E/R_E$,

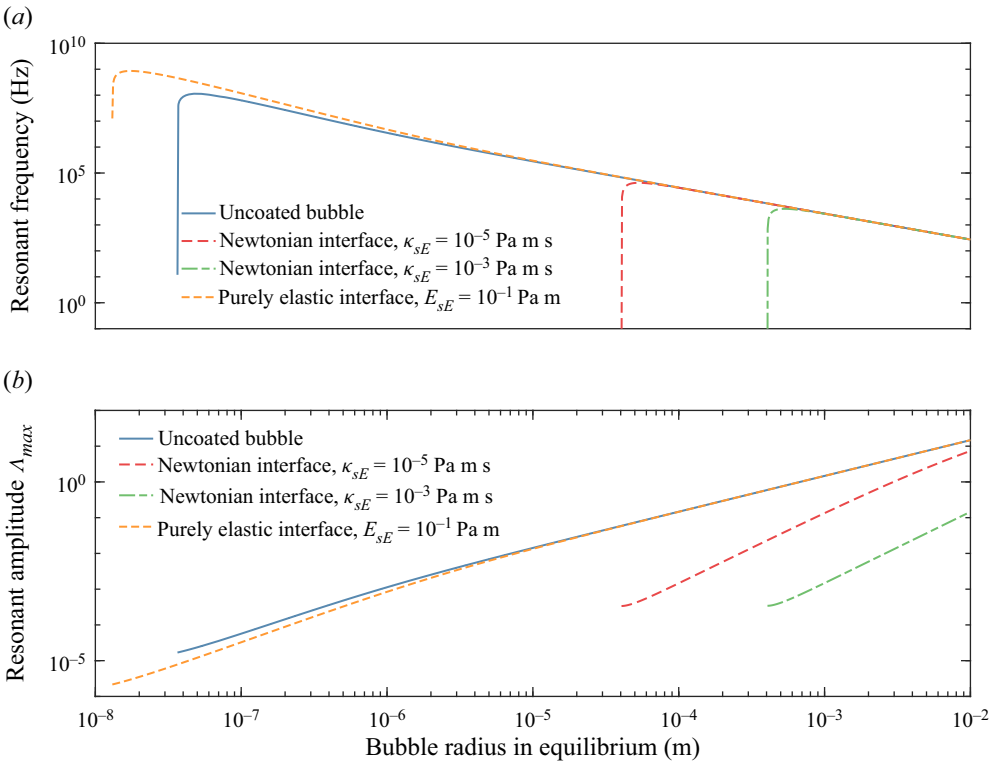

Figure 11. Effects of surface dilatational viscosity and dilatational elasticity on the resonant frequency and resonant amplitude. Here $\varepsilon = 0.001$, $\mu = 0.001$ Pa s, $\gamma_E = 0.052$ N m^{-1} and $\chi = 0$ are used.

the surface dilatational elasticity or the relaxation time has minor effects on oscillations, which will bring difficulties to experiments.

5. Conclusions

We have developed a model for bubble dynamics in a protein solution, including varying surface tension and dynamic adsorption/desorption of protein onto the bubble surface. We use the Maxwell model to describe the protein-coated bubble surface because the gas–liquid interface with an adsorbed protein layer is usually viscoelastic (Narsimhan 2016). If the surface relaxation time goes to zero, then our derived formula for a viscoelastic bubble surface reduces to the Boussinesq–Scriven constitutive equation for a Newtonian interface, which is suitable for a surfactant- or lipid-coated bubble (Chatterjee & Sarkar 2003; Marmottant *et al.* 2005).

We have studied two cases to understand the importance of surface rheology. In the first case study, in which the bubble dissolves in a protein solution, we find that the protein reduces the dissolution rate of the bubble. If we ignore the situation of buckling and protein shedding, the dissolution can be divided into three processes: (1) inertio-capillary process, in which the rate of dissolution is determined by the Weber number (the ratio of gas inertial force to the surface tension force); (2) inertio-elasto-capillary process, in which the surface excess stress counteracts the surface tension force such that the dissolution rate reduces; and (3) elasto-capillary process, in which the surface excess stress balances the surface tension force, and the dissolution rate is governed by both the protein desorption rate

and the elasto-capillary number (the ratio of surface tension to the surface dilatational elasticity). If the protein-coated bubble surface has a high dilatational elasticity and a large relaxation time, the surface excess stress will quickly grow and balance the surface tension force such that the first two processes can be neglected; in that case, the dissolution rate can be predicted by (3.7). Suppose we have experimental data for the bubble radius with respect to time; we can use (3.7) to fit the experimental data and find the protein desorption rate, surface relaxation time and surface dilatational elasticity.

If a large clean bubble is formed in a protein solution, the dissolution rate is negligible. Hence the protein adsorption rate is determined by the protein diffusion coefficient in the bulk solution D_c and the protein adsorption/desorption ability (θ^a and θ^d). If the bubble dissolution rate is not negligible compared with the protein adsorption rate, the reduction of the surface area increases the protein concentration on the bubble surface. After the protein concentration on the bubble surface Γ reaches the equilibrium value, $\Gamma_{eq} = \theta^a c_\infty/(\theta^a c_\infty + \theta^d)$. If the protein desorption rate is small compared with the bubble dissolution rate, the protein mass on the bubble will remain almost constant, i.e. the protein concentration on the bubble continues growing as the bubble shrinks. If the protein desorption rate is large, then the protein concentration on the bubble surface will satisfy the adsorption isotherm. In other words, $\Gamma = \Gamma_m$ if the protein diffusion coefficient D_c is small; and $\Gamma = \Gamma_{eq}$ if the protein diffusion rate in the bulk solution is large compared with the dissolution rate.

In the second case study, in which a small fluctuating pressure drives a protein-coated bubble to oscillate, we have derived a formula for the oscillation at the steady state. We find that the surface dilatational viscosity contributes to bubble damping, while the surface dilatational elasticity contributes to bubble stiffness. Although we cannot obtain an explicit solution for the resonant frequency in the general case, we get the explicit solution for a bubble with a Newtonian interface (surface relaxation time goes to zero) or an elastic interface (surface relaxation time goes to infinity). We also find a critical frequency (greater than the natural frequency of an uncoated bubble), beyond which including the surface dilatational elasticity and the surface dilatational viscosity enlarges the amplitude of oscillation.

Our model is applicable for globular proteins. For the fibrillar structure of proteins, the molecules at the interface can have different conformations, and hence the protein adsorption isotherms (2.15) and (2.17) need to be modified or replaced with appropriate expressions. Additionally, our model is valid if the concentrations are below the critical micelle concentration of conventional non-ionic/ionic surfactants in the presence of salt, or below the critical aggregation concentration of proteins. If the concentrations are above the critical micelle concentration or the critical aggregation concentration, the solutions contain monomers and micelles/aggregates, and we need an additional equation to describe the kinetics of micelles/aggregates (Patist *et al.* 2002; Craster *et al.* 2009; Morris, Watzky & Finke 2009). Moreover, conventional surfactants usually have a large desorption rate; thus, the bubble under shrinkage can remain spherical when the surfactant concentration on the bubble surface is close to the maximum possible concentration. However, if the protein adsorption is close to the maximum possible adsorption, the fast shrinkage of the bubble usually leads to a non-spherical bubble shape (the bubble volume decreases while the bubble surface area remains constant) since the protein desorption rate is low. Thus, our results are qualitative for relatively large concentrations of protein solutions.

Our findings in the first case study indicate that the Maxwell model can characterize the protein-coated bubble surface. Also, surface rheology can be important and needs to

receive more attention. Additionally, our theoretical derivation for the dissolution rate and the bubble response to an acoustic pressure provide a way to predict the properties of a viscoelastic bubble surface. This work provides insight into protein-coated bubbles and helps guide the design of protein-coated bubbles, which are used as vehicles to deliver drugs, as active miniature tracers to probe the rheology of soft and biological materials (Dollet *et al.* 2019), or as contrast agents to enhance the ultrasound backscatter in ultrasonic imaging (Dauba *et al.* 2020).

Funding. This research was supported by a grant from the Eli Lilly and Company.

Declaration of interests. The authors report no conflict of interest.

Author ORCIDs.
Xiaoxu Zhong https://orcid.org/0000-0001-5790-1895;
Arezoo M. Ardekani https://orcid.org/0000-0003-3301-3193.

References

Alvarez, N.J., Walker, L.M. & Anna, S.L. 2010*a* Diffusion-limited adsorption to a spherical geometry: the impact of curvature and competitive time scales. *Phys. Rev.* E **82**, 011604.

Alvarez, N.J., Walker, L.M. & Anna, S.L. 2010*b* A microtensiometer to probe the effect of radius of curvature on surfactant transport to a spherical interface. *Langmuir* **26** (16), 13310–13319.

Brennen, C.E. 2013 *Cavitation and Bubble Dynamics*. Cambridge University Press.

Brennen, C.E. 2015 Cavitation in medicine. *Interface Focus* **5** (5), 20150022.

Chatterjee, D. & Sarkar, K. 2003 A Newtonian rheological model for the interface of microbubble contrast agents. *Ultrasound Med Biol.* **29** (12), 1749–1757.

Church, C.C. 1988 Prediction of rectified diffusion during nonlinear bubble pulsations at biomedical frequencies. *J. Acoust. Soc. Am.* **83** (6), 2210–2217.

Craster, R.V., Matar, O.K. & Papageorgiou, D.T. 2009 Breakup of surfactant-laden jets above the critical micelle concentration. *J. Fluid Mech.* **629**, 195–219.

Crum, L.A. 1984 Rectified diffusion. *Ultrasonics* **22** (5), 215–223.

Cui, P., Zhang, A.-M., Wang, S. & Khoo, B.C. 2018 Ice breaking by a collapsing bubble. *J. Fluid Mech.* **841**, 287–309.

Dauba, A., Delalande, A., Kamimura, H.A.S., Conti, A., Larrat, B., Tsapis, N. & Novell, A. 2020 Recent advances on ultrasound contrast agents for blood-brain barrier opening with focused ultrasound. *Pharmaceutics* **12** (11), 1125.

Doinikov, A.A. & Dayton, P.A. 2007 Maxwell rheological model for lipid-shelled ultrasound microbubble contrast agents. *J. Acoust. Soc. Am.* **121** (6), 3331–3340.

Dollet, B., Marmottant, P. & Garbin, V. 2019 Bubble dynamics in soft and biological matter. *Annu. Rev. Fluid Mech.* **51** (1), 331–355.

Edwards, D.A., Brenner, H. & Wasan, D.T. 1991 *Interfacial Transport Processes and Rheology*. Butterworth-Heinemann.

Epstein, P.S. & Plesset, M.S. 1950 On the stability of gas bubbles in liquid–gas solutions. *J. Chem. Phys.* **18** (11), 1505–1509.

Fainerman, V.B., Lucassen-Reynders, E.H. & Miller, R. 1998 Adsorption of surfactants and proteins at fluid interfaces. *Colloids Surf.* A **143** (2), 141–165.

Fujikawa, S. & Akamatsu, T. 1980 Effects of the non-equilibrium condensation of vapour on the pressure wave produced by the collapse of a bubble in a liquid. *J. Fluid Mech.* **97** (3), 481–512.

Hanwright, J., Zhou, J., Evans, G.M. & Galvin, K.P. 2005 Influence of surfactant on gas bubble stability. *Langmuir* **21** (11), 4912–4920.

Jin, F., Balasubramaniam, R. & Stebe, K.J. 2004 Surfactant adsorption to spherical particles: the intrinsic length scale governing the shift from diffusion to kinetic-controlled mass transfer. *J. Adhes.* **80** (9), 773–796.

Kapodistrias, G. & Dahl, P.H. 2012 Scattering measurements from a dissolving bubble. *J. Acoust. Soc. Am.* **131** (6), 4243–4251.

Keller, J.B. & Miksis, M. 1980 Bubble oscillations of large amplitude. *J. Acoust. Soc. Am.* **68** (2), 628–633.

Khan, A.H. & Dalvi, S.V. 2020 Kinetics of albumin microbubble dissolution in aqueous media. *Soft Matt.* **16**, 2149–2163.

KLOEK, W., VAN VLIET, T. & MEINDERS, M. 2001 Effect of bulk and interfacial rheological properties on bubble dissolution. *J. Colloid Interface Sci.* **237** (2), 158–166.

KWAN, J.J. & BORDEN, M.A. 2012 Lipid monolayer collapse and microbubble stability. *Adv. Colloid Interface Sci.* **183–184**, 82–99.

LANGEVIN, D. 2014 Rheology of adsorbed surfactant monolayers at fluid surfaces. *Annu. Rev. Fluid Mech.* **46** (1), 47–65.

LIGER-BELAIR, G., CILINDRE, C., GOUGEON, R.D., LUCIO, M., GEBEFÜGI, I., JEANDET, P. & SCHMITT-KOPPLIN, P. 2009 Unraveling different chemical fingerprints between a champagne wine and its aerosols. *Proc. Natl Acad. Sci.* **106** (39), 16545–16549.

LIN, G.L., PATHAK, J.A., KIM, D.H., CARLSON, M., RIGUERO, V., KIM, Y.J., BUFF, J.S. & FULLER, G.G. 2016 Interfacial dilatational deformation accelerates particle formation in monoclonal antibody solutions. *Soft Matt.* **12**, 3293–3302.

LIU, R.H., YANG, J., PINDERA, M.Z., ATHAVALE, M. & GRODZINSKI, P. 2002 Bubble-induced acoustic micromixing. *Lab Chip* **2** (3), 151–157.

LYONS, J.J., HANEY, M.M., FEE, D., WECH, A.G. & WAYTHOMAS, C.F. 2019 Infrasound from giant bubbles during explosive submarine eruptions. *Nat. Geosci.* **12**, 952–958.

MANIKANTAN, H. & SQUIRES, T.M. 2020 Surfactant dynamics: hidden variables controlling fluid flows. *J. Fluid Mech.* **892**, P1.

MARMOTTANT, P., VAN DER MEER, S., EMMER, M., VERSLUIS, M., DE JONG, N., HILGENFELDT, S. & LOHSE, D. 2005 A model for large amplitude oscillations of coated bubbles accounting for buckling and rupture. *J. Acoust. Soc. Am.* **118** (6), 3499–3505.

MILLER, R., FAINERMAN, V.B., MAKIEVSKI, A.V., KRÄGEL, J., GRIGORIEV, D.O., KAZAKOV, V.N. & SINYACHENKO, O.V. 2000 Dynamics of protein and mixed protein/surfactant adsorption layers at the water/fluid interface. *Adv. Colloid Interface Sci.* **86** (1), 39–82.

MOONEY, M. 1951 The viscosity of a concentrated suspension of spherical particles. *J. Colloid Sci.* **6** (2), 162–170.

MORRIS, A.M., WATZKY, M.A. & FINKE, R.G. 2009 Protein aggregation kinetics, mechanism, and curve-fitting: a review of the literature. *Biochim. Biophys. Acta Proteins Proteomics* **1794** (3), 375–397.

MURAKAMI, K., YAMAKAWA, Y., ZHAO, J., JOHNSEN, E. & ANDO, K. 2021 Ultrasound-induced nonlinear oscillations of a spherical bubble in a gelatin gel. *J. Fluid Mech.* **924**, A38.

NARSIMHAN, G. 2016 Characterization of interfacial rheology of protein-stabilized air–liquid interfaces. *Food Engng Rev.* **8**, 367–392.

PATIST, A., KANICKY, J.R., SHUKLA, P.K. & SHAH, D.O. 2002 Importance of micellar kinetics in relation to technological processes. *J. Colloid Interface Sci.* **245** (1), 1–15.

PEÑAS-LÓPEZ, P., PARRALES, M.A., RODRÍGUEZ-RODRÍGUEZ, J. & VAN DER MEER, D. 2016 The history effect in bubble growth and dissolution. Part 1. Theory. *J. Fluid Mech.* **800**, 180–212.

PLESSET, M.S. 1949 The dynamics of cavitation bubbles. *J. Appl. Mech.* **16** (3), 277–282.

PLESSET, M.S. & PROSPERETTI, A. 1977 Bubble dynamics and cavitation. *Annu. Rev. Fluid Mech.* **9** (1), 145–185.

PLESSET, M.S. & ZWICK, S.A. 1954 The growth of vapor bubbles in superheated liquids. *J. Appl. Phys.* **25** (4), 493–500.

POULICHET, V. & GARBIN, V. 2015 Cooling particle-coated bubbles: destabilization beyond dissolution arrest. *Langmuir* **31** (44), 12035–12042.

PROSPERETTI, A. & LEZZI, A. 1986 Bubble dynamics in a compressible liquid. Part 1. First-order theory. *J. Fluid Mech.* **168**, 457–478.

RAYLEIGH, LORD 1917 VIII. On the pressure developed in a liquid during the collapse of a spherical cavity. *London Edinburgh Dublin Phil. Mag. J. Sci.* **34** (200), 94–98.

SHARMA, V., JAISHANKAR, A., WANG, Y.-C. & MCKINLEY, G.H. 2011 Rheology of globular proteins: apparent yield stress, high shear rate viscosity and interfacial viscoelasticity of bovine serum albumin solutions. *Soft Matt.* **7**, 5150–5160.

STONE, H.A. 1990 A simple derivation of the time-dependent convective-diffusion equation for surfactant transport along a deforming interface. *Phys. Fluids* A*: Fluid Dyn.* **2** (1), 111–112.

TOMAR, D.S., KUMAR, S., SINGH, S.K., GOSWAMI, S. & LI, L. 2016 Molecular basis of high viscosity in concentrated antibody solutions: strategies for high concentration drug product development. *mAbs* **8** (2), 216–228.

VEILLEUX, J.-C., MAEDA, K., COLONIUS, T. & SHEPHERD, J.E. 2018 Transient cavitation in pre-filled syringes during autoinjector actuation. In *Proceedings of the 10th International Symposium on Cavitation (CAV2018)*. ASME Press.

VINCENT, O., MARMOTTANT, P., QUINTO-SU, P.A. & OHL, C.-D. 2012 Birth and growth of cavitation bubbles within water under tension confined in a simple synthetic tree. *Phys. Rev. Lett.* **108**, 184502.

WANG, S.S., JIAO, Z.J., HUANG, X.Y., YANG, C. & NGUYEN, N.T. 2009 Acoustically induced bubbles in a microfluidic channel for mixing enhancement. *Microfluid Nanofluid* **6**, 847–852.

WARNEZ, M.T. & JOHNSEN, E. 2015 Numerical modeling of bubble dynamics in viscoelastic media with relaxation. *Phys. Fluids* **27** (6), 063103.

YBERT, C. & DI MEGLIO, J.-M. 1998 Study of protein adsorption by dynamic surface tension measurements: diffusive regime. *Langmuir* **14** (2), 471–475.

ZHANG, Y., DOU, Z., VEILLEUX, J.-C., SHI, G.H., COLLINS, D.S., VLACHOS, P.P., DABIRI, S. & ARDEKANI, A.M. 2021 Modeling cavitation bubble dynamics in an autoinjector and its implications on drug molecules. *Intl J. Pharm.* **608**, 121062.

ZHONG, X., ESHRAGHI, J., VLACHOS, P., DABIRI, S. & ARDEKANI, A.M. 2020 A model for a laser-induced cavitation bubble. *Intl J. Multiphase Flow* **132**, 103433.